OCEANBOX WHITE PAPER 01 v1

MODEL SETUP AND VALIDATION

Frank Gaardsted, Ole Anders Nøst, Stig Rune Jensen, Hilde Iversen, Jonas Juselius & Svenn Hanssen

November 2024

Oceanbox AS (Org.nr: 928 178 056)
Kløvervegen 17, 9015 Tromsø, NORWAY

Oceanbox - Model setup and validation

Frank Gaardsted, Ole Anders Nøst, Stig Rune Jensen,
Hilde Iversen, Jonas Juselius and Svenn Hanssen

November 2024

Contents

Preface

Oceanbox would like to thank Salmar, Aqua Kompetanse and Aquafuture for valuable input to the model validation part of this report. Salmar provided measurements from 13 sites and Aquafuture provided data from 1 site. Aqua Kompetanse assisted in the processing of the raw data from the about half of the sites.

Summary

This report gives an overview of the technical setup of the hydrodynamic model and particle tracking model that form the core of the Oceanbox online services. The quality of the hydrodynamic model results is discussed based on comparisons with current and temperature measurements.

Oceanbox uses a hydrodynamic model with an unstructured grid (Finite Volume Community Ocean Model, FVCOM), which makes it an ideal model for complicated coastlines because it provides the possibility of varying grid resolution. The Oceanbox model resolution for the Norwegian coast ranges from 800m at the boundary in the open ocean, to 30m-40m around aquaculture sites and narrow straits. Currently (November 2024), the Oceanbox model system covers the Norwegian coast from Rogaland to Finnmark.

The particle tracking model uses the results from FVCOM and allows users to perform dispersion simulations directly in the online map. The particle model is a Lagrangian model which tracks the movement of numerical particles as if they were transported by the current field produced by FVCOM. By implementing various properties for the particles (i.e. vertical movement, growth rate, mortality), the dispersion pattern of different types of actual physical material can be simulated. Currently, Oceanbox has modules for simulation of passive transport, virus particles, salmon lice and deposition of organic waste from fish farms.

The quality of the hydrodynamic model was evaluated by comparison of model results to in situ current and temperature measurements from a total of 14 sites in Nordmøre and Trøndelag. Approx. 4000 days of data were included in the analysis. There was no overall systematic deviation between the model and the measurements for average daily median and daily maximum current speed and daily average temperature. This includes no depth dependency in the deviations and no temporal trend in the deviations. Identifying the reason for the deviations that occasionally do occur is difficult, but the data indicate that the largest deviations in speed are linked to a few sites. Inspection of the details around the sites suggests that small inaccuracies in the model bathymetry may be responsible. This highlights the importance of accurately resolving the coastline and bathymetry to accurately model the near-field circulation around fish farms.

Chapter 1

Introduction

The role of hydrodynamic modeling in Norwegian coastal zone management has gradually increased in recent decades, primarily as a response to the need for improved tools to address issues related to a rapidly growing aquaculture industry. The most well known example is the implementation of the national NorKyst800 modeling system ([2], [1]) which covers the entire Norwegian coast. Modeling services have also become a part of the product line of several of the private companies involved in marine environmental consulting. Nevertheless, there are still challenges that prevent the utilization of modeling tools in many cases that would clearly benefit from them. The main challenge is the complexity of such models and the high competence requirements of setting up and running them on a large scale.

Oceanbox is a software company that builds on previous modeling developments and aims to push them further by dramatically increasing the availability and efficiency of modeling services (Figure 1.1). The core of the Oceanbox system is a traditional model setup, centered around a high resolution hydrodynamic model providing detailed current maps of the ocean. The datasets produced by this setup is integrated into an online web application which allows users to rapidly and easily visualize the data and to carry out further dispersion calculations based on the modeled current fields. More infornation about the Oceanbox services is available at www.oceanbox.io

The purpose of this report is:

1. To provide a technical overview of the parts of the Oceanbox system that are involved in producing the actual results, i.e. the hydrodynamic model (currents, salinity and temperature) and the particle tracking model (dispersion patterns).

2. To assess the overall quality of the Oceanbox-model system through comparison of model results with in situ measurements. The main focus has been on detecting any overall systematic problems in the model setup, but examples from single sites have been included to illustrate how local conditions can influence the results.

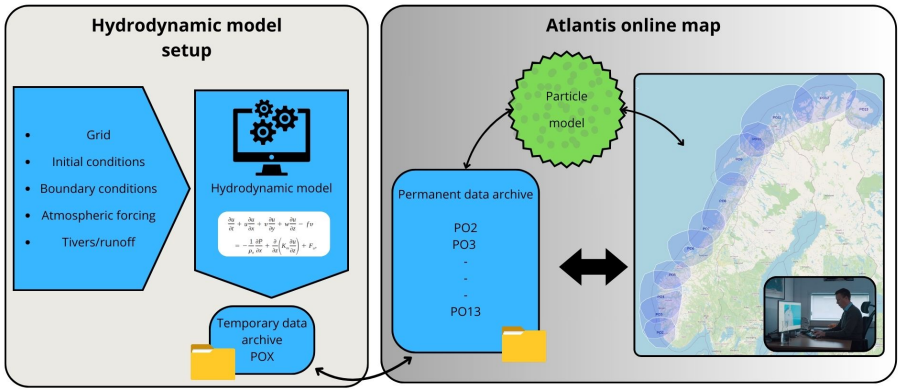

Figure 1.1: *The Oceanbox modeling system can be divided into two main components: 1 (left): The simulation of current fileds with a hydrodynamic model and 2 (right): The online user interface which allows users to interact with the data. This includes both visualization and online dispersion simulations through the use of the built in particle tracking model. The purpose of this report is to describe the hydrodymamic model setup (1) and the particle tracking model.*

The hydrodynamic model along with forcing and input data is described in Section 2, the particle model is described in Section 3. Based on comparison with in situ current measurements, the quality of the model is discussed in Section 4.

Chapter 2

Model setup

2.1 Hydrodynamic model

The main challenge when modeling the Norwegian coast is the complicated coastline combined with the need to cover large areas. This is especially true in aquaculture related problems, where the sites have relatively small horizontal extent and are often located close to shore, and pathogens of interest (virus, lice) can survive for days and weeks and thus be transported large distances with the currents. To accurately model the water transport to and from a site therefore requires that both the near-field and far-field circulation are reasonably accurate.

Oceanbox uses the Finite Volume Community Ocean Model (FVCOM, [10]) to perform hydrodynamic simulations in this challenging scenario. FVCOM has a triangular unstructured grid, which has the ability to vary the resolution within the model domain, and the triangles can be fitted smoothly to an irregular coastline. The variable resolution makes it possible to use high resolution where it is most needed and coarser resolution where this is acceptable. This makes it possible to model large region while simultaneously resolving the complex coastline.

FVCOM has been used in numerous studies of coastal and estuarine waters [9, 14–16, 28] and also globally and in the Arctic Ocean [8, 30]. FVCOM uses an unstructured triangular grid in the horizontal and terrain-following σ coordinates in the vertical [10]. The model solves the equations for momentum and mass conservation as well as the equations for temperature, salinity, and density.

Oceanbox currently has 12 model setups along the coast of Norway, from Rogaland to Finnmark. Each model is designed to cover one of the 13 production areas used in Norwegian salmon aquaculture management. The focus in this report is on Nordmøre and Trøndelag (Production Area 6 (PO6) and Production Area 7 (PO7), Figure 2.1), but all the models use the same input data sources and grid resolution structure. Each of the grids extend well beyond

the boundaries of its production area, and is constructed to have the highest resolution in narrow straits and around aquaculture locations inside the production area. The finest resolution in these areas is around 30-40 m and becomes coarser towards open water areas. At the boundary towards the open ocean the resolution is 800 m.

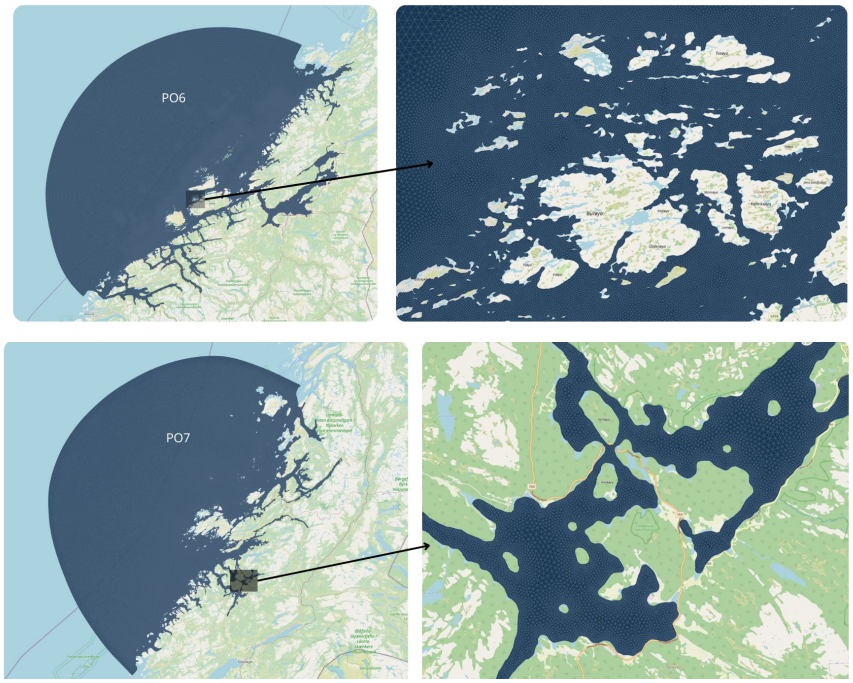

Figure 2.1: *Model domains for PO6 (top) and PO7 (bottom). The left panels show the full grid and the right panels show a subsection of the grid.*

2.2 Model input data

The FVCOM model depends on a wide range of input data to be set up in a specific location. Along the Norwegian coast these data are available via various public national organizations such as the Norwegian Meteorological Institute, the Norwegian Mapping Authorities and The Norwegian Water Resources and Energy Directorate.

Input data sources:

- **Initial and boundary conditions**. The initial conditions and boundary conditions of the Oceanbox models are interpolated from the Norwegian Meteorological Institute NorShelf model setup [27]. This is a data-assimilated model system that provides hourly values of physical oceano-

graphic variables for the entire Norwegian coast with a resolution of 2.4 km. Oceanbox uses current velocity, surface elevation salinity and temperature from the NorShelf model as input to our models

- **Atmospheric forcing**. Atmospheric forcing data are interpolated onto the FVCOM grid from the AROME MetCoop weather modeling system [19]. The AROME MetCoop model system is run by the Norwegian Meteorological Institute.

- **Coastline and bathymetry data**. The Oceanbox model grids are built based on the best available coastline and bathymetry data (up to 50 m resolution) from the Norwegian Mapping Authority.

- **River runoff data**. Data on river runoff are collected from an operational service run by the Norwegian Water Resources and Energy Directorate (NVE). NVE divides the Norwegian coast into 247 catchment areas and derives daily runoff values for each catchment. We call these main catchment areas. The derived values for the main catchments are based on observed and modeled runoff, and the methods are described by Beldring et al. [3, 4] and Petterson et al. [26]. The total runoff from a main catchment is distributed to the different rivers and streams. The NVE dataset identifies the catchment area associated with each of the largest rivers. The runoff from these large rivers is given by $Q_r = Q_m A_r / A_m$, where Q_r is the river runoff, Q_r is the total runoff in the main catchment, A_r is the area of the river catchment and A_m is the area of the main catchment. When runoff from the large rivers is derived, the remaining runoff from the main catchment is evenly distributed among the remaining rivers and streams. The NVE dataset is extremely detailed, and one model domain may contain a few thousand river outlets.

Chapter 3

Particle tracking model

3.1 Advection model

The Drifters particle tracking model is an offline Lagrangian model, where the 3D velocity fields used for guiding the individual particles' motion are precomputed at hourly snapshots on an unstructured triangular grid using the ocean circulation model FVCOM. The field values are evaluated at each particle's position and at each propagation time step using one of the interpolation methods described below and used in either a simple Euler forward stepping model or a 4th order Runge-Kutta scheme. The model time step is typically chosen much smaller than the snapshot frequency of the driving velocity fields, usually in the range of a few seconds to a few minutes, for which a linear time interpolation of the velocity field is done for intermediate time steps between the snapshots.

3.2 Field interpolation

Several different types of interpolation are necessary to convert the static snapshots of gridded oceanographic data into the continuous and dynamic fields used for particle propagation. The interpolation is done in three independent parts: one for time (t), one for the vertical (z) and one for the combined horizontal (x,y) dimensions. The interpolation in time and in the vertical are always linear, meaning a gradual transition from one time step to the next, and between sigma levels in the vertical coordinate. In the horizontal plane there are a few different options available depending on the context: the simplest version is to use a constant value inside each grid element (meaning no interpolation); second, a linear interpolation using barycentric coordinates can be used, leading to a field that is continuous in the field value, but not its derivative, across cell boundaries; and finally, a second-order Clough-Tocher interpolation scheme can be used, resulting in a field that is continuous both in its value and its first derivative across cell boundaries. As one might expect, each level of sophistication leads

to a smoother field, but at the cost of increasing computational complexity.

3.3 Boundary conditions

Particles can encounter four kinds of boundary, and their behavior at such encounters can be modeled in different ways. In the horizontal plane, the particles can approach the modeled domain's edge either at a land boundary or at the boundary towards open sea, while in the vertical direction the particle can reach the surface or the seabed.

At the horizontal boundary, the particle can take one of four different actions:

- Strand: The particle gets stuck at the boundary. It will remain in the model visually and it will continue to contribute to the computed particle concentration fields, but it will never be re-emitted into the ocean for further propagation.
- SkipStep: The particle will remain at its current (horizontal) position inside the model domain and will wait for the next time step. If the velocity field changes to a direction that is no longer pushing the particle on land, it will continue its motion along the new current direction. The vertical motion will always be sustained, even if the horizonal motion is skipped. This is to allow for up/down-welling effects to carry the particle into potential outward flowing currents, e.g. at river outlets.
- ReduceStep: The time step of the model is recursively reduced until the particle is no longer driven on shore by the velocity field. In principle, it should always be possible to avoid particle stranding by sufficiently reducing the time step in this way, since the underlying velocity field should not have any component leading out of the model domain. In practice, however, one might reach a practical limit for this time step, in which case the behavior is changed to SkipStep instead of further time step reduction.
- Remove: The particle is fully removed from the simulation and will no longer appear visually or contribute to any particle concentration fields.

At the surface vertical boundary, the behavior is always equivalent to the seabed Glide action, but with vertical axis inverted. At the open boundary, the typical behavior is Remove, but at the land and seabed boundaries, either of the options can be useful depending on the situation.

3.4 Particle release

Simulation particles are released with a random uniform distribution within a vertically oriented cylinder of a given radius and height, given as center depth and a variance (z +/- dz). The particles are initially spread evenly to fill the

entire cylinder, regardless of any model boundaries, be it land, open, seabed or surface. If any particle happens to be created beyond any of these boundaries, it will immediately suffer the effects of the appropriate boundary action that is used for the simulation (see boundary conditions above).

In a continuous release scenario, N particles are emitted every hour, and the particles are evenly distributed both in space (within the cylinder), but also in time (within each hour).

3.5 Model types

3.5.1 Transport model

The Transport simulation type is the simplest particle model, where the particles do not have any intrinsic properties or capabilities. The particles will drift passively with the 3D ocean currents, and will remain in the simulation for unlimited time, unless encountering an absorbing boundary condition. Propagation backwards in time is allowed, by setting a negative time step.

Default parameters for the Transport advection model are:

- Time step: 300 sec
- Time integration: RungeKutta
- Time interpolation: Linear
- Open boundary: Remove
- Land boundary: SkipStep
- Seabed boundary: Glide

3.5.2 Virus model

In the Virus simulation type, the particle motion is passive drift along the 3D ocean current, but each particle will have a limited life span within the simulation. This life span can be modeled either as a hard cutoff at some maximum allowed age, and/or as a random process through a daily mortality rate in which each particle is given a fixed probability of surviving each simulation day. Propagation backwards in time is allowed by setting a negative time step.

Default parameters for the Virus advection model are:

- Time step: 300 sec
- Time integration: RungeKutta
- Time interpolation: Linear
- Vertical interpolation: Linear
- Horizontal interpolation: Clough-Tocher

- Open boundary: Remove
- Land boundary: SkipStep
- Seabed boundary: Glide

3.5.3 Sedimentation model

In the Sedimentation simulation type, each particle is given a vertical settling velocity which is added on top of the background drift from the modeled 3D ocean current. The settling velocity of each particle is chosen in a two-step procedure: first, each particle is assigned to one of a discrete set of size categories based on a user-defined probability distribution. Each size category maps to a continuous velocity interval, again user-defined; second, within this velocity interval, a random specific velocity is chosen for each particle based on a flat uniform probability. Once each particle is given its unique settling velocity at creation, it remains constant throughout the simulation.

Due to the typically high settling velocities, relative to the background vertical motion, it is important to set the propagation time step significantly smaller for sedimentation simulations than for the typical horizontally dominated passive drift models. This is to avoid the particle passing through several vertical layers in a single time step, potentially missing important horizontal velocity fluctuations along the way. The use of a simple Euler forward stepping model allows for a decoupling of the constant vertical settling motion from the background velocity field motion, since the vertical displacement is easily computed in a single point. In contrast, a constant settling velocity is not easily modeled along a path trajectory, as is necessary in the Runge-Kutta model, due to the terrain-following vertical sigma-coordinate used in the ocean circulation model (a constant settling velocity in the real-world depth parameter z corresponds to a space-varying settling velocity along a path using a terrain-following sigma-coordinate system). For this reason, the Sedimentation module uses the simpler Euler particle propagation scheme, but this is compensated for by significantly reducing the time step down to 5 seconds.

In addition to the constant settling and the dynamic background velocity, a vertical diffusion contribution is added to account for sub-grid turbulent motion. This contribution is modeled as a standard random walk process using a diffusion coefficient of 0.01 m2/s. This vertical diffusion process is a key component in the re-suspension model described below, as it drives the re-entrainment of deposited particles back into the above ocean currents after they have been released from the ocean floor in a re-suspension event.

The seabed boundary condition for Sedimentation models is set to Deposit, in which particles stick to the seabed upon contact. The further fate of the deposited particle will depend on other model parameters. In the simplest case, without re-suspended activated, the particle is immediately accounted for in the computed sedimentation field, and then taken out of the simulation.

In the case when re-suspension is activated, the deposited particle will remain inactive at the seabed until the end of each macro-cycle (typically one hour,

based on the snapshot frequency of the oceanographic data). Between each macro-cycle, all deposited particles are checked for a re-suspension event, by computing the bottom shear stress, which depends on the current velocity on the bottom-most layer. If the stress exceeds a user-defined critical shear threshold, the particle is marked as re-suspended before entering the micro-cycles of the advection model, of which the first step is the vertical diffusion process where the particles will gain a random vertical displacement which allows for the particle to be re-entrained into the ocean circulation above (the diffusion process is symmetric, so half the particles will gain a downward displacement which means it will remain deposited within the next macro-cycle). If the particle is re-deposited at a later stage, it will again wait to the end of the following macro-cycle, and the process is repeated until the particle's age exceeds a user-defined consolidation time.

At each macro-cycle, all currently deposited particles are accounted for on a 2D sedimentation field on the seabed, representing the rate of deposition at the current snapshot. In the case of no re-suspension, each particle is counted exactly once, and then removed from the simulation. In the case where re-suspension is activated, every particle will contribute to a fixed number of snapshots, given by the consolidation time and snapshot frequency, and the particle's weight will be evenly distributed among all the snapshots. If a deposited particle is not re-suspended between two macro-cycles, its weight will accumulate in its current position. Increasing the consolidation time will allow more mobility for each particle but will add to the computational load.

When a time series of sedimentation rate snapshots are computed, the total amount of deposited sediments can be accumulated for the entire simulation period. Initially, the particle release and sedimentation rate snapshots will be normalized for each day, and it is only at the post-processing step of accumulation that the actual amount of released matter is specified, be it fish feed/feces or other non-biological materials. The release rate can then be given either as a fixed amount that is kept constant throughout the simulation period, or as a time series of variable output with arbitrary temporal resolution. The separation of the model into a normalized particle propagation part (computationally expensive) and a post-processing step with analysis (computationally cheap) allows for the possibility of experimenting with different release strategies, e.g. with different feeding plans throughout a fish farm's production cycle.

Default parameters for the Sedimentaton advection model are:

- Time step: 5 sec
- Time integration: Euler
- Time interpolation: Linear
- Vertical interpolation: Linear
- Horizontal interpolation: Linear
- Open boundary: Remove

- Land boundary: Strand
- Seabed boundary: Deposit

Chapter 4

Hydrodynamic Model validation

4.1 Current and temperature measurements

Through collaboration with customers and partners, Oceanbox has access to a fairly extensive dataset of current measurements in the area from Nordmøre to Trøndelag. In the Norwegian framework for salmon aquaculture management (2024), the measurements were carried out in Production Area 6 (PO6) and Production Area 7 (PO7). Data from a total of 14 locations in PO6 (6 locations) and PO7 (8 locations) have been available for this study. The positions are shown in Figure 4.1, and more details is presented in Table 4.1.

The measurements were carried out in connection with existing aquaculture sites or in connection with the planning of possible future sites, and therefore the measurement setup met the requirements for such measurements, typically NS 9415:2021 [24], NS 9425-2:2003 [25], and NS 9425-1:1999 [23]. This means that the measurement periods in most cases varied between 1 - 3 months and that the measurement depths were from the near surface layer (5m to 15m), bottom layer and midway between the bottom and the lower edge of the fish cages. The instruments also had temperature sensors that recorded the temperature throughout the deployment period. A detailed description of the data for each of the instrument moorings and a presentation of the results can be found in the corresponding reports listed in Table 4.1. The measurements were carried out over the period from May 2022 to January 2024. Together, the data set adds up to a total of 4701 days of current data and 3113 days of temperature data.

Table 4.1: *Overview of current and temperature measurements. The measurements were carried out in connection with existing or possible future aquaculture sites. The names of the sites as well as reference to the corresponding technical data report (where available) are given in column 1. The measurement period and position are given in columns 2 an 3 respectively. Measurement depths are given in column 5. The bottom depth at each location is given in the last column. Where multiple current measurement depths are listed in a single line, measurements were done with a profiling current meter capable of measuring many depth layers simultaneously. In these cases, data from 8m and 15m were used in this study. If the temperature measurement depth was different than the current measurement, it is listed in brackets. Additional information about the instrument moorings can be found in the technical reports.*

Site	Time	Position		Measurement depth (m)	Bottom depth (m)
		Latitude	Longitude		
Kattholmen [5]	02.07.22 - 12.09.22	63°52.250‘N	008°40.771‘W	8, 15 (26)	60
	26.10.22 - 28.11.22	63°52.334‘N	008°40.690‘W	5	65
	26.10.22 - 28.11.22	63°52.334‘N	008°40.690‘W	15	65
Rataren [6]	02.07.22 - 20.09.22	63°46.903‘N	008°30.915‘W	8, 15 (24)	44
	20.09.22 - 14.11.22	63°54.068‘N	008°32.146‘W	5	47
	20.09.22 - 14.11.22	63°54.068‘N	008°32.146‘W	15	47
	14.11.22 - 22.12.22	63°54.068‘N	008°32.146‘W	5	47
	14.11.22 - 22.12.22	63°54.068‘N	008°32.146‘W	15	47
	26.01.23 - 17.04.23	63°54.068‘N	008°32.146‘W	5	47
	26.01.23 - 17.04.23	63°54.068‘N	008°32.146‘W	15	47
Salatskjæra [18]	29.11.22 - 17.04.23	63°54.392‘N	008°35.416‘W	8, 15 (22)	55
Steinnesa [29]	19.07.22 - 02.09.22	63°54.068‘N	008°32.146‘W	8	50
	19.07.22 - 02.09.22	63°54.068‘N	008°32.146‘W	19	50
	21.10.22 - 28.11.22	63°54.068‘N	008°32.146‘W	5	50
	02.09.22 - 28.11.22	63°54.068‘N	008°32.146‘W	15	50
	19.07.22 - 13.10.22	63°54.068‘N	008°32.146‘W	35	50
	19.07.22 - 13.10.22	63°54.068‘N	008°32.146‘W	47	50
Sørøyflesa [7]	12.02.22 - 12.07.22	63°59.050‘N	009°03.372‘W	8, 15 (21)	46
Ørnøya [17]	24.08.22 - 26.10.22	63°45.619‘N	008°26.716‘W	5	28
	14.12.22 - 26.01.23	63°45.619‘N	008°26.716‘W	5	28
	24.08.22 - 26.10.22	63°45.619‘N	008°26.716‘W	15	28
	26.10.22 - 29.11.22	63°45.660‘N	008°26.683‘W	15	27
	02.09.22 - 21.10.22	63°45.619‘N	008°26.716‘W	28	28
Dolma [32]	15.02.23 - 06.06.23	65°01.561‘N	011°40.837‘W	8, 15 (32)	110
	06.06.23 - 08.09.23	65°01.561‘N	011°40.837‘W	8, 15 (32)	110
Dolma [31]	15.02.23 - 08.06.23	65°01.520‘N	011°40.056‘W	8, 15 (32)	89
	15.02.23 - 21.03.23	65°01.520‘N	011°40.056‘W	57	89
	15.02.23 - 21.03.23	65°01.520‘N	011°40.056‘W	88	89
Gimlingsundet -	23.11.22 - 11.01.23	65°12.527‘N	011°58.524‘W	8, 15 (30)	66
	11.01.23 - 25.02.23	65°12.527‘N	011°58.524‘W	8, 15 (30)	66
	23.11.22 - 11.01.23	65°12.527‘N	011°58.524‘W	42	66
	11.01.23 - 25.02.23	65°12.527‘N	011°58.524‘W	42	66
	23.11.22 - 11.01.23	65°12.527‘N	011°58.524‘W	64	66
	11.01.23 - 25.02.23	65°12.527‘N	011°58.524‘W	64	66
Kvingra [12]	26.04.23 - 03.08.23	65°12.032‘N	011°34.211‘W	8, 15 (31)	152
	03.08.23 - 08.11.23	65°12.032‘N	011°34.211‘W	8, 15 (29)	152
Purkholmen [13]	31.08.23 - 31.10.23	64°48.376‘N	010°34.256‘W	8, 15 (29)	64
	31.08.23 - 31.10.23	64°48.376‘N	010°34.256‘W	40	64
	31.08.23 - 31.10.23	64°48.376‘N	010°34.256‘W	63	64
Purkholmen -	29.10.23 - 29.01.24	64°48.376‘N	010°34.256‘W	8, 15 (31)	64
	29.10.23 - 29.01.24	64°48.376‘N	010°34.256‘W	40	64
	29.10.23 - 29.01.24	64°48.376‘N	010°34.256‘W	63	64
Risværgalten [22]	03.05.22 - 03.08.22	64 °57.912‘N	011°32.158‘W	8 , 15 (31)	95
	03.05.22 - 09.06.22	64 °57.912‘N	011°32.158‘W	94	95
Smineset [20]	04.05.22 - 03.08.22	64 °45.398‘N	011°32.439‘W	8, 15 (28)	120
	04.05.22 - 20.06.22	64 °45.398‘N	011°32.439‘W	69	120
	04.05.22 - 20.06.22	64 °45.398‘N	011°32.439‘W	119	120
Ternskjæret [21]	04.05.22 - 20.06.22	64°46.717‘N	011°38.414‘W	8, 15 (33)	163
	20.60.22 - 03.08.28	64°46.717‘N	011°38.414‘W	8, 15 (31)	110
	04.05.22 - 20.06.22	64°46.717‘N	011°38.414‘W	77	163
	04.05.22 - 20.06.22	64°46.717‘N	011°38.414‘W	128	163

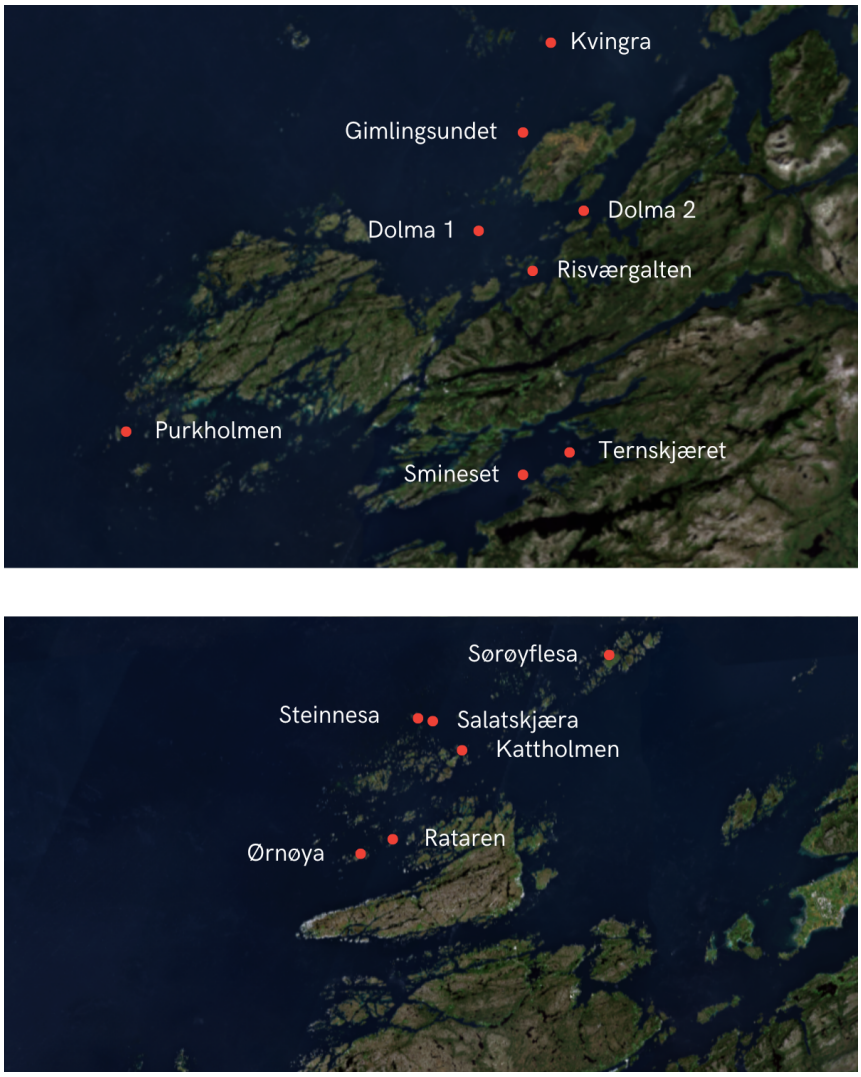

Figure 4.1: *Current measurement locations in PO7 (top) and PO6 (bottom). Exact positions are given in Table 4.1.*

4.2 Model data

To be able to compare the model data and the measurement data side by side, model data was extracted from the nearest grid point, horizontally and vertically, for each of the measurement positions and measurement periods in Table 4.1. Due to the relatively high resolution of the grid (30 - 40m) around fish farms, the distance between the measurement positions and the model data positions did not exceed about 20m.

4.3 Data analysis

Ocean currents are highly variable with respect to both speed and direction, and it can be difficult to summarize the deviation in model performance in a simple metric. In many cases, where the amount of available data is not too large, graphical visualizations such as histograms of speed and direction, along with simple time series plots, may be the best approach. In cases where the amount of data makes it overwhelming to inspect everything visually, some sort of statistical metric is necessary. Attempts have been made to summarize the deviation between the models and measurements in a single metric ([11]), but a lot of nuances are lost in this approach.

In this report we have chosen to use a combination of statistics and visualization of the raw data. To keep it simple, we have limited the statistical analysis to computation of the daily median, maximum, and minimum values of current speed, and daily mean values of temperature. In addition, rose-plots and qq-plots have been included for a few individual sites to show the typical model quality at the local level.

4.4 Results

The distributions for the median and maximum current speeds largely overlap, but in both cases the model distributions were wider and slightly skewed to the right with more values in the higher range, while the measurement distributions were narrower and more symmetrical (Figure 4.2). However, the mean values were similar in both cases (Table 4.2). On average, the daily median speed was 8.2 cm/s in the measurements and 10.5 cm/s in the model. The corresponding values for average daily maximum speeds were 20.3 cm/s and 20.0 cm/s for the measurements and model, respectively. Minimum daily current speeds were generally very low in the measurements (less than 5 cm/s) and consistently slightly higher in the model. The daily mean minimum speed was 0.8 cm/s in the measurements and 3.8 cm/s in the model.

Table 4.2: *Summary statistics based on analysis of the 4701 daily time series of current speed from both measurements and model.*

	Measurements				**Model**			
	Mean	Max	Min	std	Mean	Max	Min	std
Daily median values	8.2	26.6	1.6	3.9	10.5	56.5	0.7	6.7
Daily max. values	20.3	52.2	3.6	8.2	20.0	69.8	1.3	11.8
Daily min. values	0.8	14.2	0.0	1.0	3.8	46.6	0.0	4.5

Figure 4.3 shows the depth distribution of the individual daily median, maximum, and minimum values. The strongest currents and the largest deviations between the measurements and the model were found in the upper 60 m of the water column. However, there was no overall depth dependency in the direction of the deviations (positive or negative), i.e. the model did not systematically over- or underestimate current speed in particular depth layers.

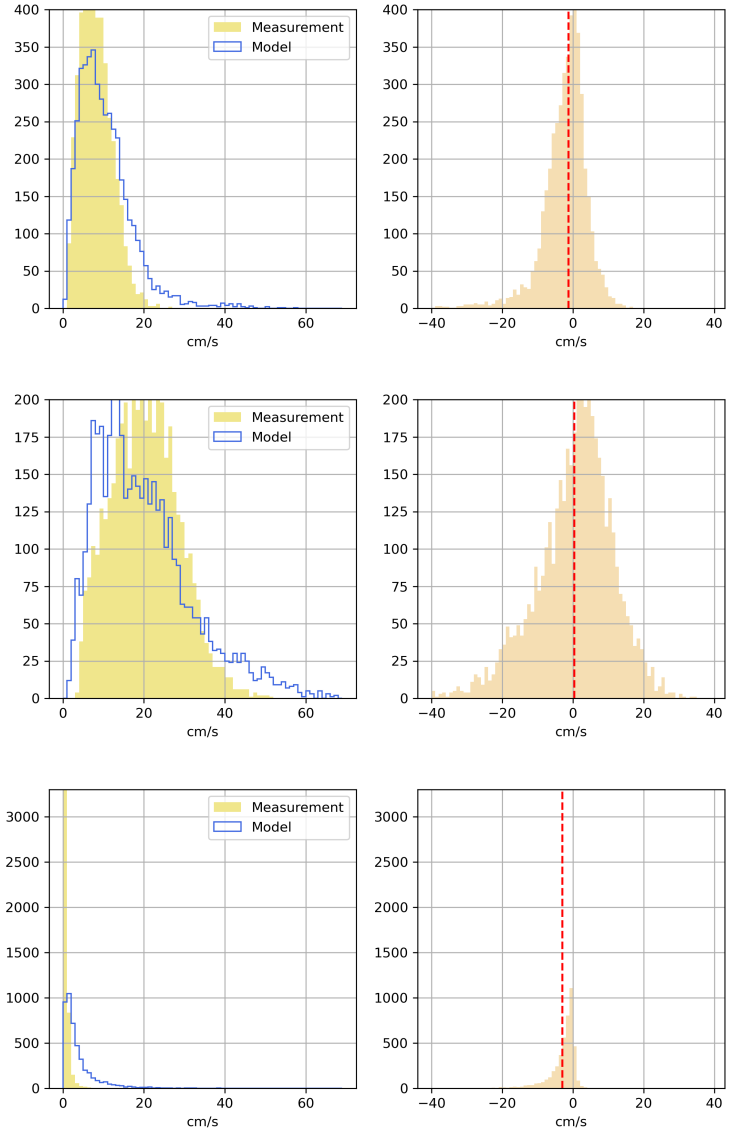

Figure 4.2: *Summary statistics based on 4701 days of current measurements from all sites and depths. Left panels: Histogram of daily median current speeds (top), daily maximum current speeds (middle) and minimum daily current speed (bottom). Right panels: Histogram of the differences between each corresponding measurement and model value for daily median current speed (top), daily maximum current speed (middle) and daily minimum current speed (bottome).*

A final view of the same speed data is shown in Figure 4.4. The plot of each daily median, maximum and minimum value as a function of time should reveal any temporal trend in the quality of the model results. There were fluctuations in the deviations, both positive and negative, but no clear overall trend of increasing deviations in either direction. The majority of the largest deviations, with stronger current speed in the model than in the measurements, did occur towards the end of the survey period. But rather than being the end point of a gradual trend, they were instead all associated with a single site, namely Purkholmen.

As both of the PO6 and PO7 model domains primarily cover areas with narrow fjords and small islands, current pathways/direction will be strongly guided by topography, and modeling current direction correctly is therefore primarily a question of model resolution and accurate coastlines. The model setup generally does this very well. In 68 % of the cases the difference between the most frequent current direction in the measurements and the model was less than or equal to 25° (Figure 4.5). In 75 % of the cases it was less than 45°. in 17 % of the cases the difference was larger than 140°, i.e. close to opposite. As the velocity at many of the sites often had two oppositely directed dominating current directions, this is in practice not necessarily indicative of a strong deviation. Ørnøya is the only site that stands out as a relatively poor site when it comes to the main current direction.

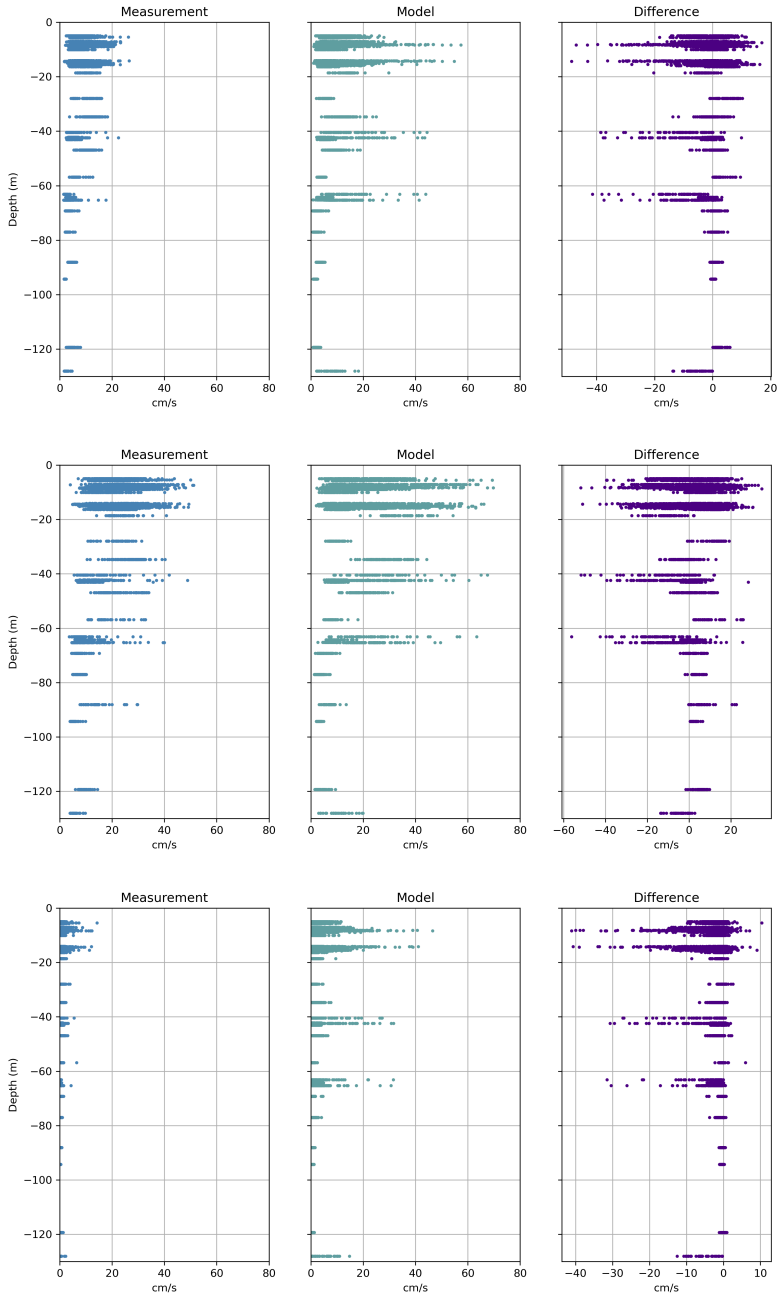

Figure 4.3: *Summary statistics based on 4701 days of current measurements. The panels in the right column show the depth distribution of the measured daily median speed (top), maximum speed (middle) and minimum speed (bottom). The corresponding statistics from the model is shown in the middle column. The pairwise differences between measurement and model are shown in the last column.*

Figure 4.4: *Time evolution of the difference between measured and modeled daily median speed (top) maximum speed (middle) and minimum speed (bottom). Data from all times and depths were included. The color and symbol of a point indicate the measurement site.*

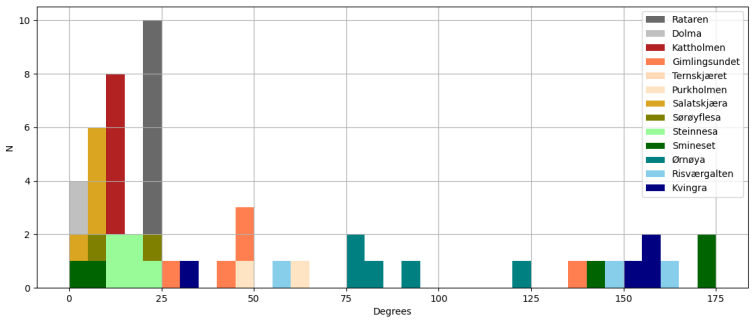

Figure 4.5: *Histogram of difference in degrees between the most frequent current directions for each data series. The bin size is 5 degrees. The analysis was done with fullt time series of raw data, i.e. no daily averaging. The larges possible difference is 180 degrees, i.e. oppositely directed currents. Site is indicated by color.*

To illustrate some of the result from the statistical analysis in more detail, a few representative examples are shown in Figure 4.6.

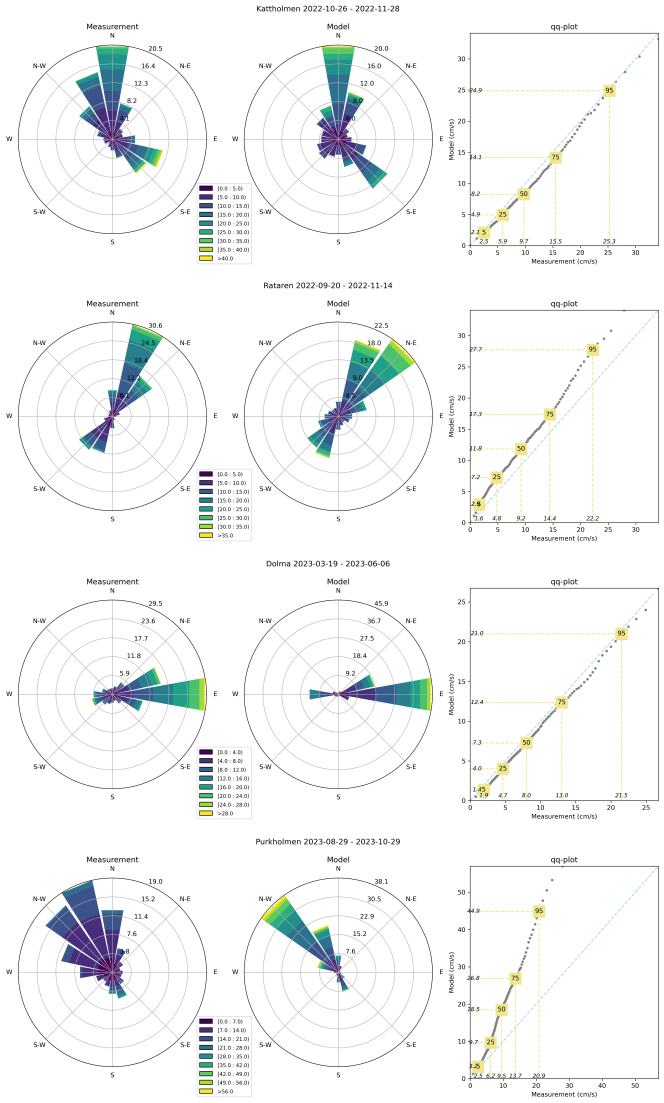

Figure 4.6: *Rose-plot for measurements (left) and model (center), and qq-plots of speed (right) for the sites Kattholmen, Rataren, Dolma and Purkholmen. The length of the sectors in the rose-plots indicate the proportion of velocity values in a given direction. The colors indicate speed classes.*

The current velocity distribution at the four sites was largely bimodal with two main directions, and this was generally reproduced in the model. This was

true even for Purkholmen, which had the largest model discrepancy in current speed. For the sites Dolma and Kattholmen, the correspondence between the model and the measurements was excellent. It was also very good for Rataren although the model had a tendency to slightly overestimate current speeds in the higher range of the speed distribution, consistent with the right-skewed speed distributions in Figure 4.2. One possible reason for the large deviations in speed at Purkholmen is the complicated bathymetry in the area of the site (Figure 4.7. At the center of the site, the bottom depth is about 37 m, but several shallow areas (appprox. 4m) can be found in the immediate vicinity of the site, and the depth is more than a 100m a short distance to the west of the site. Due to smoothing of model bathymetry, this degree of bathymetry complexity is not resolved in the model, which has a smoother bottom profile in the area around Purkholmen (not shown). Similarly, the deviation in direction at Ørnøya appears to be linked to smoothing of bathymetry.

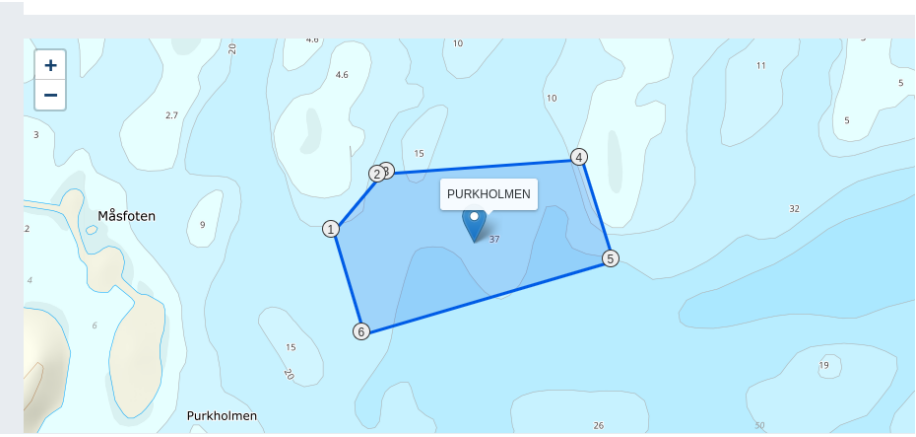

Figure 4.7: *Bathymetry in the area around Purkholmen*

The distributions of daily mean temperature for the measurements and the model are shown in Figure 4.8. The distribution for both the measurement distribution and the model distribution was bimodal, reflecting generally warmer water in the summer months vs. winter months. The deviations between the measurements and the model ranged from about -4 to 2.5 degrees C, but the average difference was only 0.1 degrees C.

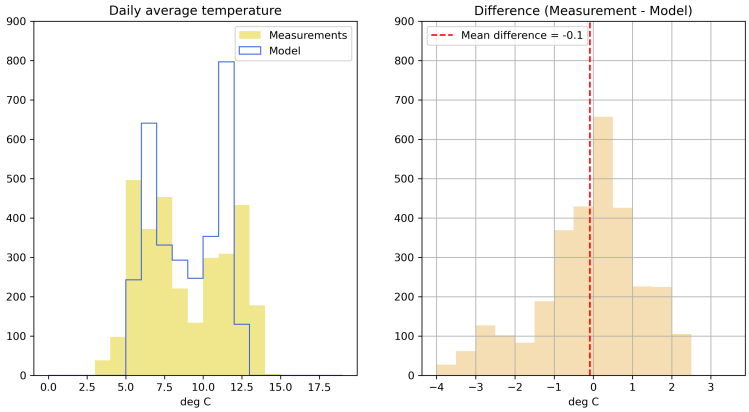

Figure 4.8: *Left: Histogram of daily mean temperature calculated from the measurements and the model. Right: The pairwise differences between measurements and model data.*

There was a slight time trend in the deviations in the daily average temperature in the sense that most of the positive differences between the measurements and the model (i.e. the model being colder, Figure 4.9) occurred in the first third of the study period. In the remaining part of the study period, the model tended to be slightly warmer than the measurements, but there was no apparent trend in the deviations if one looks at the final year of the simulation in isolation.

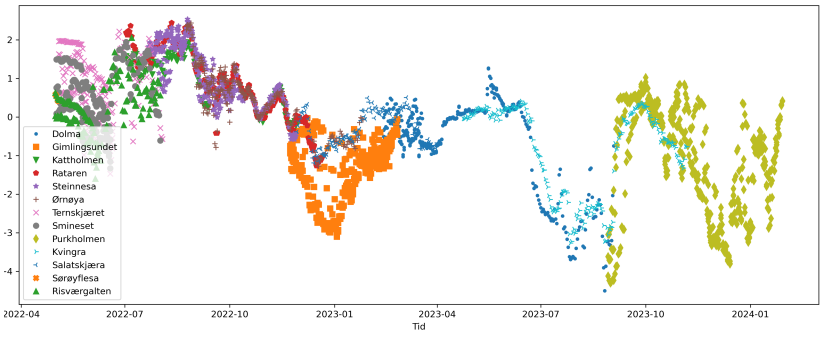

Figure 4.9: *Time evolution of the difference between measured and modeled daily mean temperature. Data from all times and depths were included. The color and symbol of a point indicate the site the data-point comes from.*

4.5 Discussion

The results presented in this report are primarily based on comparisons of daily statistical speed and temperature values from the model results and measurements. Discrepancies between the model and the measurements can be the result of a wide range of factors, and determining the reason for any deviation is not necessarily easy. In some cases, it can be due to systematic problems that affect the whole model domain, e.g. problems with forcing data, or problems with the model formulation (advection scheme, parameterizations, etc.) In other cases, the model setup may generally be good, but still underperform in certain areas, e.g. because of insufficient resolution to accurately include complicated geographical features. Finally, there can be undetected problems with the measurements, which make the model results seem worse than they actually are.

In this report, we have compared the model results with measurements from actual aquaculture sites, i.e., from locations relatively close to shore. The measurements used here were collected from 14 different geographical positions, from a wide range of depths, and over a time span covering all seasons. The fact that many of the sites clearly are very well represented in the model (Figure 4.6), and that the daily statistical values from the measurements and the model are comparable, indicate that the overall model setup performs well. There were some deviations between the model and the measurements, but since no depth dependency in deviations was found and since there was no obvious trend in the time development of the deviations, it seems unlikely that there are general systematic problems with the setup.

However, the comparison does highlight the importance of having accurate bathymetry and coastline in the model setup. This basically comes down to having an adequate resolution. Local geography greatly influences the current

circulation close to shore and in relatively shallow areas, and must therefore be considered carefully in grid design and smoothing of bathymetry.

It is difficult to know if model validation from different model domains would produce similar results, but Oceanbox's model setups from the other areas along the Norwegian coast use the same forcing and input sources as the ones presented here.

Bibliography

[1] Lars Asplin, Jon Albretsen, Ingrid Askeland Johnsen, and Anne Dagrun Sandvik. The hydrodynamic foundation for salmon lice dispersion modeling along the norwegian coast. *Ocean dynamics*, 70(8):1151–1167, 2020.

[2] Lars Asplin, Anne Dagrun Sandvik, and Jon Albretsen. Kystmodellen norkyst-800–en strømmodell for hele norskekysten. Technical report, Havforskningsinstituttet, 2011.

[3] S Beldring, LA Roald, and A Voksø. Avrenningskart for norge. årsmiddelverdier for avrenning 1961-1990. *Map of annual runoff for Norway for the period 1961-1990.) Norwegian Water Resources and Energy Directorate, Document*, (2):49, 2002.

[4] Stein Beldring, Kolbjørn Engeland, Lars A Roald, Nils Roar Sælthun, and Astrid Voksø. Estimation of parameters in a distributed precipitation-runoff model for norway. *Hydrology and Earth System Sciences*, 7(3):304–316, 2003.

[5] Øystein Breiteig. SR-SF-Kattholmen-110202119-3011-01-00. Technical report, Åkerblå, 2022.

[6] Øystein Breiteig. SR-SF-Rataren-110202176-3011-01-001. Technical report, Åkerblå, 2023.

[7] Øystein Breiteig and Anne Kari Meisingset. Sr-1120-sf-sørøyflesa-101767-01-002. Technical report, Åkerblå, 2022.

[8] Changsheng Chen, Guoping Gao, Yu Zhang, Robert C Beardsley, Zhigang Lai, Jianhua Qi, and Huichan Lin. Circulation in the arctic ocean: Results from a high-resolution coupled ice-sea nested global-fvcom and arctic-fvcom system. *Progress in Oceanography*, 141:60–80, 2016.

[9] Changsheng Chen, Zhaolin Lin, Robert C Beardsley, Tom Shyka, Yu Zhang, Qichun Xu, Jianhua Qi, Huichan Lin, and Danya Xu. Impacts of sea level rise on future storm-induced coastal inundations over massachusetts coast. *Natural Hazards*, 106(1):375–399, 2021.

[10] Changsheng Chen, Hedong Liu, and Robert C Beardsley. An unstructured grid, finite-volume, three-dimensional, primitive equations ocean model: application to coastal ocean and estuaries. *Journal of atmospheric and oceanic technology*, 20(1):159–186, 2003.

[11] Stig B Dalsøren, Jon Albretsen, and Lars Asplin. New validation method for hydrodynamic fjord models applied in the Hardangerfjord, Norway. *Estuarine, Coastal and Shelf Science*, 246:107028, 2020.

[12] Hege G. Frøysa. Vannstrømmåling ved kvingra, leka kommune, april–november 2023. 2208-11-23s v.2. Technical report, Aqua Kompetanse, 2023.

[13] Hege G. Frøysa. Vannstrømmåling ved purkholmen, nærøysund kommune, august–oktober 2023. 2524-10-23s v. Technical report, Aqua Kompetanse, 2023.

[14] Zhigang Lai, Ronghua Ma, Guangyin Gao, Changsheng Chen, and Robert C Beardsley. Impact of multichannel river network on the plume dynamics in the p earl r iver estuary. *Journal of Geophysical Research: Oceans*, 120(8):5766–5789, 2015.

[15] Zhigang Lai, Ronghua Ma, Mingfen Huang, Changsheng Chen, Yong Chen, Congbin Xie, and Robert C Beardsley. Downwelling wind, tides, and estuarine plume dynamics. *Journal of Geophysical Research: Oceans*, 121(6):4245–4263, 2016.

[16] Chunyan Li, Wei Huang, Changsheng Chen, and Huichan Lin. Flow regimes and adjustment to wind-driven motions in lake pontchartrain estuary: A modeling experiment using fvcom. *Journal of Geophysical Research: Oceans*, 123(11):8460–8488, 2018.

[17] Aleksander Libæk. Sr-sf-Ørnøya-110202240-3011-01-001. Technical report, Åkerblå, 2023.

[18] Anne Kari Meisingset. SR-SF-Salatskjæra-110200438-3011-01-001. Technical report, Åkerblå, 2023.

[19] Malte Müller, Mariken Homleid, Karl-Ivar Ivarsson, Morten AØ Køltzow, Magnus Lindskog, Knut Helge Midtbø, Ulf Andrae, Trygve Aspelien, Lars Berggren, Dag Bjørge, et al. Arome-metcoop: A nordic convective-scale operational weather prediction model. *Weather and Forecasting*, 32(2):609–627, 2017.

[20] Benedicte Otterdal Nergaard. Vannstrømmåling ved smineset n, namsos kommune, mai-august 2022. 1398-8-22s. Technical report, Aqua Kompetanse, 2022.

[21] Benedicte Otterdal Nergaard. Vannstrømmåling ved ternskjæret ii, namsos kommune, mai-august 2022. 1403-8-22s. Technical report, Aqua Kompetanse, 2022.

[22] Benedicte Otterdal Nergaard. Vannstrømmåling ved risværgalten, nærøysund kommune, januar-februar 2012 og mai-august 2022. 1404-8-22s. Technical report, Aqua Kompetanse, 2023.

[23] Standard Norge. Del 1: Strømmålinger i faste punkter. NS 9425:1999. Technical report, Standard Norge, 1999.

[24] Standard Norge. Flytende akvakulturanlegg-lokalitetsundersøkelse, prosjektering, utførelse og bruk. NS 9415:2021. Technical report, Standard Norge, 2021.

[25] Standard Norge. Oseanografi-del 2: Strømmålinger ved hjelp av adcp. NS 9425-2:2003. Technical report, Standard Norge, 2023.

[26] Lars-Evan Pettersson. Totalavløpet fra norges vassdrag 1900-2010. *Norwegian Water Resources and Energy Directorate (NVE). Rapport*, pages 39–2012, 2012.

[27] Johannes Röhrs, Ann Kristin Sperrevik, and Kai H Christensen. Norshelf: A reanalysis and data-assimilative forecast modelfor the norwegian shelf sea. Technical report, Tech. Rep. ISSN 2387-4201 04/2018, Norwegian Meteorological Institute, doi . . . , 2018.

[28] Yunfang Sun, Changsheng Chen, Robert C Beardsley, Dave Ullman, Bradford Butman, and Huichan Lin. Surface circulation in block island sound and adjacent coastal and shelf regions: A fvcom-codar comparison. *Progress in Oceanography*, 143:26–45, 2016.

[29] Tore Magnus Arnesen Taklo. SR-SF-Steinnesa-110202181-3011-01-001. Technical report, Åkerblå, 2022.

[30] Yu Zhang, Changsheng Chen, Robert C Beardsley, Guoping Gao, Zhigang Lai, Beth Curry, Craig M Lee, Huichan Lin, Jianhua Qi, and Qichun Xu. Studies of the canadian arctic archipelago water transport and its relationship to basin-local forcings: Results from ao-fvcom. *Journal of Geophysical Research: Oceans*, 121(6):4392–4415, 2016.

[31] Judith Øhlberg, Thu. Vannstrømmåling ved dolma, nærøysund kommune, februar–juni 2023. 2048-6-23s v.2. Technical report, Aqua Kompetanse, 2023.

[32] Judith Øhlberg, Thu. Vannstrømmåling ved dolma, nærøysund kommune, februar–september 2023. 2048-9-23s v.2. Technical report, Aqua Kompetanse, 2023.